PNAS RESEARCH ARTICLE | MICROBIOLOGY

Gut metabolite L-lactate supports *Campylobacter jejuni* population expansion during acute infection

Ritam Sinha[a], Rhiannon M. LeVeque[a], Sean M. Callahan[b,1], Shramana Chatterjee[a], Nejc Stopnisek[a,2], Matti Kuipel[c], Jeremiah G. Johnson[b], and Victor J. DiRita[a,3]

Edited by Andreas Baumler, University of California, Davis, CA; received September 22, 2023; accepted November 15, 2023

How the microaerobic pathogen *Campylobacter jejuni* establishes its niche and expands in the gut lumen during infection is poorly understood. Using 6-wk-old ferrets as a natural disease model, we examined this aspect of *C. jejuni* pathogenicity. Unlike mice, which require significant genetic or physiological manipulation to become colonized with *C. jejuni*, ferrets are readily infected without the need to disarm the immune system or alter the gut microbiota. Disease after *C. jejuni* infection in ferrets reflects closely how human *C. jejuni* infection proceeds. Rapid growth of *C. jejuni* and associated intestinal inflammation was observed within 2 to 3 d of infection. We observed pathophysiological changes that were noted by cryptic hyperplasia through the induction of tissue repair systems, accumulation of undifferentiated amplifying cells on the colon surface, and instability of HIF-1α in colonocytes, which indicated increased epithelial oxygenation. Metabolomic analysis demonstrated that lactate levels in colon content were elevated in infected animals. A *C. jejuni* mutant lacking *lctP*, which encodes an L-lactate transporter, was significantly decreased for colonization during infection. Lactate also influences adhesion and invasion by *C. jejuni* to a colon carcinoma cell line (HCT116). The oxygenation required for expression of lactate transporter (*lctP*) led to identification of a putative thiol-based redox switch regulator (LctR) that may repress *lctP* transcription under anaerobic conditions. Our work provides better insights into the pathogenicity of *C. jejuni*.

Campylobacter jejuni | ferret model | lactate | inflammation

Significance

There is a gap in knowledge about the mechanisms by which *Campylobacter jejuni* populations expand during infection. Using an animal model which accurately reflects human infection without the need to alter the host microbiome or the immune system prior to infection, we explored pathophysiological alterations of the gut after *C. jejuni* infection. Our study identified the gut metabolite L-lactate as playing an important role as a growth substrate for *C. jejuni* during acute infection. We identified a DNA binding protein, LctR, that binds to the *lctP* promoter and may repress *lctP* expression, resulting in decreased lactate transport under low oxygen levels. This work provides greater insights into *C. jejuni* pathogenicity.

Foodborne diseases are important threats in both developed and developing countries. Among the more prevalent foodborne bacterial pathogens is *Campylobacter jejuni*, annually responsible for an estimated 1.5 million cases of gastroenteritis (1). With the emergence of antibiotic-resistant strains, the choice of antibiotic to treat these infections may soon be limited; the US Centers for Disease Control and Prevention considers drug-resistant *Campylobacter* infection as a serious threat (2, 3). Common symptoms of gastroenteritis mediated by *C. jejuni* are diarrhea (sometimes bloody), fever, vomiting, and abdominal cramps. Symptoms typically begin within 2 to 5 d after infection and last about a week. *C. jejuni* gastroenteritis can be a more persistent, and even life-threating, infection in immunocompromised patients such as those with AIDS or hypogammaglobulinemia (3, 4). It can also have the serious postinfection sequelae of Guillain–Barré syndrome (5). The precise mechanisms of its pathogenicity remain uncertain as *C. jejuni* does not encode pathogenicity islands associated with secretion of toxins or other effectors that would enable it to manipulate host cell biology or survive intracellularly, as do other gastrointestinal pathogens such as *Salmonella*, *Shigella*, and *Vibrio cholerae* (6–8). More well-studied pathogens such as facultative anaerobes in the family *Enterobacteriaceae*, including *Citrobacter rodentium* and *Salmonella typhimurium*, induce crypt colonic hyperplasia via virulence factors, and regulate mucosal epithelial oxygenation and lactate concentration in the gut during inflammation, which influence their growth and pathogenicity (6, 9).

Lack of an ideal animal model means that there remain gaps in understanding the precise mechanism of *C. jejuni* disease progression in vivo. Some questions regarding *C. jejuni* pathogenicity that remain unanswered are the following: i) How does *C. jejuni* establish its niche and expand in the gut lumen during the inflammatory stage of infection? ii) How does *C. jejuni* compete with the gut microbiota for colonization in gut? iii) What is the major carbon source for *C. jejuni* growth during acute infection?

Our main goal is to understand environmental conditions during infection that influence colonization and population expansion of *C. jejuni*. We used a ferret-infection model to investigate pathogenicity of *C. jejuni*. This model has several advantages over currently used mouse models, including no required antibiotic treatment or other manipulation of the gut microbiota prior to infection (10), or disarming key components of the immune system such as MyD88 (11), NF-kB (12), or IL-10 (13). Like in human infections, ferret

Author contributions: R.S. and V.J.D. designed research; R.S., R.M.L., S.M.C., S.C., N.S., and M.K. performed research; R.S., M.K., J.G.J., and V.J.D. analyzed data; and R.S., J.G.J., and V.J.D. wrote the paper.

The authors declare no competing interest.

This article is a PNAS Direct Submission.

[1]Present address: Department of Cell and Developmental Biology, Smilow Center for Translational Research, Perelman School of Medicine, University of Pennsylvania, Philadelphia, PA 19104.

[2]Present address: Department of Microbial Ecology, Netherlands Institute of Ecology, 6700 AB Wageningen, The Netherlands.

[3]To whom correspondence may be addressed. Email: diritavi@msu.edu.

This article contains supporting information online at https://www.pnas.org/lookup/suppl/doi:10.1073/pnas.2316540120/-/DCSupplemental.

Published January 3, 2024.

infections by *C. jejuni* are characterized by rapid growth within 2 to 3 d of infection, severe inflammatory responses, and pathophysiological changes in the gastrointestinal tract (10). Absent significant manipulation, mouse models of *C. jejuni* infection lack these features.

In this study, we assessed the disease dynamics of *C. jejuni* in 5- to 6-wk-old ferrets, investigating colonization, localization patterns, and pathophysiological changes in the gut during early and acute stage of infection after orogastric inoculation with *C. jejuni.* We describe changes of gut microbiota and metabolites during the acute (inflammatory) stage of infection. We identified L-lactate as a potential carbon source for growth, and we demonstrate that the lactate transporter operon (*lctP*) is essential for *C. jejuni* expansion and colonization in the inflamed gut. Finally, we identified a potential redox switch regulator (LctR) of *lctP* which, we hypothesize, in its oxidized state comes off the *lctP* promoter enabling lactate uptake and growth in the inflamed gut.

Results

***C. jejuni* Grows in the Ferret Gut during Inflammation.** Experimental infection of humans and primates with *C. jejuni* have used oral doses as high as 10^9 to 10^{10} CFU to achieve infection and acute illness, although infection may occur with much lower doses during outbreaks (14, 15). To test dose-dependent infection by *C. jejuni* in ferrets, aged 5- to 6-wk old animals were infected with two different doses, 10^8 or 10^9 CFU/mL, of *C. jejuni* strain 11168 and *C. jejuni* loads in feces were determined and pathophysiological changes in the colon were scored by histological analysis. At the higher dose of infection animals shed approximately 10^7 CFU/g of stool after 24 h, as compared to 5×10^4 CFU/g of stool from animals infected at the lower dose. Animals infected at the higher dose shed approximately 10^7 CFU/g of stool after 24 h, as compared to 5×10^4 CFU/g of stool from animals infected at the lower dose. By 72 h, animals infected at the higher dose exhibited increased shedding of *C. jejuni*, to nearly 10^{10} CFU/g of stool, while those infected at the lower dose were shedding only slightly higher numbers of *C. jejuni* than they were at 24 h (no *C. jejuni* were detected in the PBS control group after 72 h of postinfection; *SI Appendix*, Fig. S1*A*). Comparative histopathological scoring analysis and H and E staining at 72 h postinfection demonstrated no histopathological differences between the PBS and the 10^8 groups but moderate to severe gastroenteritis signs in the 10^9 group (epithelial cell damage, inflammatory cell infiltration, goblet cell depletion, cryptic hyperplasia and cryptic abscess) (*SI Appendix*, Fig. S1 *B* and *C*). Analysis with anti-*Campylobacter* antibody identified many *C. jejuni* near colonic epithelial cells in animals infected with the higher dose, whereas *C. jejuni* was present only within the colonic lumen area in animals infected with the lower dose (*SI Appendix*, Fig. S1*B*). These findings indicate that inoculation with 10^9 CFU of *C. jejuni* 11168 causes infection and acute gastroenteritis after 72 h in ferrets, which is like what is observed for human campylobacteriosis (14, 16). These data also suggest that intestinal inflammation supports *C. jejuni* expansion in ferret gut, similar to how intestinal inflammation induces the growth of facultative anaerobes such as *Escherichia coli*, *Salmonella enterica sv.* Typhimurium and *Citrobacter rodentium* (6, 9).

We investigated other pathophysiological changes during the acute stage of *C. jejuni* infection to explore potential determinants of its growth. We infected ferrets with 5×10^9 CFU/mL of *C. jejuni* strain 11168 and measured bacterial levels in colon, small intestine, mesenteric lymph node (MLN), liver, and spleen days one and three postinfection. Levels of *C. jejuni* at every site were higher on day 3 postinfection compared to day 1, with the highest concentration in the colon, where *C. jejuni* levels rose from approximately 10^6 cfu/g of tissue on day 1 to approximately 10^{10} cfu/g on day 3 (Fig. 1*A*). Expansion of *C. jejuni* in the colon on day 3 was also confirmed by 16sRNA sequencing (Fig. 1*B*). Although we did not explore it further, the presence of *C. jejuni* in deeper tissue such as liver and spleen on day 3 is evidence of systemic infection in the ferret.

As *C. jejuni* levels were highest in the colon, we focused on the molecular mechanisms of colonization and inflammatory signs in this site. Analysis with anti-*Campylobacter* antibody identified sparse clusters of *C. jejuni* present within the colonic lumen area on day 1; in contrast, day 3 sections demonstrated much greater levels of *C. jejuni* closely associated with colonic epithelial cells and detectable in crypts, like in human infection (Fig. 1*C*) (16). To measure the intracellular burden of *C. jejuni* on day three after infection, we used a gentamicin protection assay previously described for *Shigella* and *Salmonella* in guinea pig and murine models, respectively (17). We incubated infected colon tissue with gentamicin, which kills extracellular bacteria, then determined colony counts of *C. jejuni* from the treated, washed tissue. After treatment, we observed approximately 10^4 cfu/g of tissue compared to approximately 10^8 cfu/g of tissue without gentamicin treatment. These data suggest that a portion of intestinal *C. jejuni* are present intracellularly (*SI Appendix*, Fig. S2 *A* and *B*), which may lead to the systemic infection observed on day 3.

Through histopathological score analysis, we observed no significant changes in the inflammatory response of mock-infected and *C. jejuni*-infected animals on day 1, whereas by day 3 postinfection, we observed signs of moderate to severe colitis in infected colon tissue (Fig. 1*D*). For example, we observed damage to the epithelial cell layer of infected tissue, infiltration of leukocytes in superficial lamina propria, and edema in infected colon tissue. This infected tissue also demonstrated evidence of crypt elongation into the gut lumen and a lower number of mucus-secreting goblet cells when compared to the mock-infected control group (Fig. 1*E*).

Increased IL-6, IL-8, and iNOS levels prime leukocyte infiltration and tissue damage, and the anti-inflammatory IL-10 knockout mouse has been used to study pathogenicity of *C. jejuni* (13). To explore the inflammatory environment further, we measured mRNA levels from genes encoding these cytokines in colon tissue of mock-infected and *C. jejuni*-infected ferrets. Infection of ferrets with *C. jejuni* led to a two- to threefold increase in transcripts encoding pro-inflammatory IL-6, IL-8, and iNOS and approximately threefold decreased levels of transcripts from the antiinflammatory IL-10 (Fig. 1*F*). From the above analysis, we conclude that *C. jejuni* causes acute infection and inflammation in this model, resulting in cryptic hyperplasia in the colon on day 3, like the acute stage of human infection (16).

During murine infection with *Citrobacterium rodentium,* cryptic hyperplasia is induced by virulence factors encoded on the locus of enterocyte effacement (LEE) (9). This induces tissue repair systems in the host, ultimately recruiting α-smooth muscle actin (α-SMA) myofibroblast cells and accumulation of undifferentiated proliferating epithelial cells (Ki67+ cells), which results in decreased numbers of goblet cells at the colon surface (9, 18). This type of tissue remodeling is associated with altered gut physiology that can support growth of the microbe. We therefore assessed whether these changes occur after *C. jejuni* infection of the ferret. Loss of goblet cells in infected tissue was observed by Alcian blue staining (Fig. 2*A*). Immunohistochemistry (IHC) on colon samples from infected and mock-infected groups using antibodies for anti-α-SMA and anti-Ki67+ antigen demonstrated α-SMA myofibroblast cells recruitment (Fig. 2*B*) and a significantly higher number of Ki67+ undifferentiated proliferated epithelial cells (Fig. 2 *C* and *D*) in the lamina

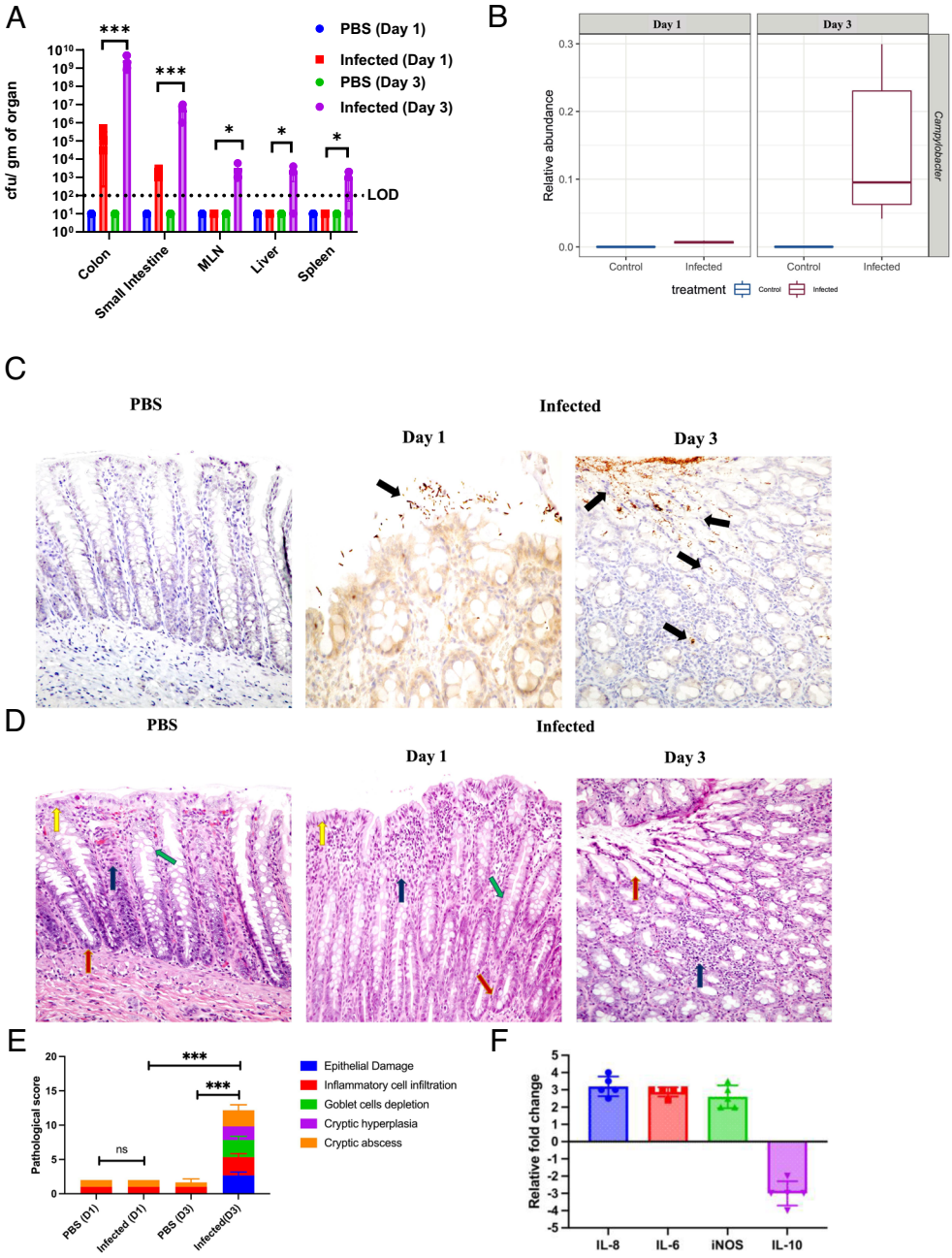

Fig. 1. Characterization of ferret as a natural disease model for *C. jejuni* pathogenesis: (*A*) *C. jejuni* 11168 WT loads were determined by CFU counts in different tissue samples day 1 and day 3 postinfection with a dose of 10^9 CFU/mL (n = 5). (*B*) The relative abundance of *C. jejuni* was determined in colonic contents day 1 and day 3 post infection by 16Sr RNA sequencing (PBS n = 3, Infected n = 6). (*C*) Immunohistochemistry (IHC) with *C. jejuni* specific antibody was performed to determine *C. jejuni* localization in colon tissue day 1 and day 3 post infection. Black arrows indicated localization of *C. jejuni* in infected colonic tissue. Representative images from two independent experiments. Original magnification, 40X. (*D*) Histology of infected and PBS-shamed ferret colonic tissue. Representative hematoxylin and eosin (H&E) stained images on day 1 and day 3 postinfection. Yellow arrow (epithelial cells), red arrows (intestinal crypts), green arrow (goblet cells), blue arrow (infiltrating leucocytes in lamina propria). Original magnification, 40X. (*E*) *C. jejuni* mediated gastroenteritis as measured by histological score of infected and uninfected (PBS) colonic tissue day 1 (D1) and day 3 (D3) postinfection (PBS n = 3, Infected n = 6). (*F*) Relative fold changes of proinflammatory (IL-8, IL-6, iNOS) and antiinflammatory (IL-10) cytokine genes determined by qRT-PCR analysis of infected colon tissue compared to that of the PBS control group (n = 5). Changes in gene expression were determined by the $2^{-\Delta\Delta CT}$ method. All error bars show ± SD. Statistical analysis was done by one-way AONOVA. *P < 0.05; **P < 0.01; ***P < 0.001; ****P < 0.000.

propria of infected colons when compared to the mock-infected control group. We conclude that the environment of the ferret gut after *C. jejuni* infection is like that of the murine intestinal tract gut that supports *C. rodentium* growth.

Metabolism of microbially derived butyrate by mature gut epithelial cells through beta-oxidation consumes oxygen, resulting in hypoxia within the gut lumen and stabilization of hypoxia inducible factor-alpha (HIF-1α) in colonocytes (19, 20). Undifferentiated proliferating cells, present mainly at the base of crypts lack β-oxidation and use aerobic respiration that produces lactate from glucose (21). These cells do not absorb oxygen and as a result, the bottom crypt areas are more oxygenated than the top of the crypts (9). With the recruitment of undifferentiated, proliferating cells on the colon surface, we hypothesized that epithelial oxygenation is increased during the acute phase stage of *C. jejuni* infection.

To test our hypothesis, we selected HIF-1α and its regulated gene claudin-1 (encoding a tight junction protein) as hypoxia indicators. These gene products are highly expressed and stabilized

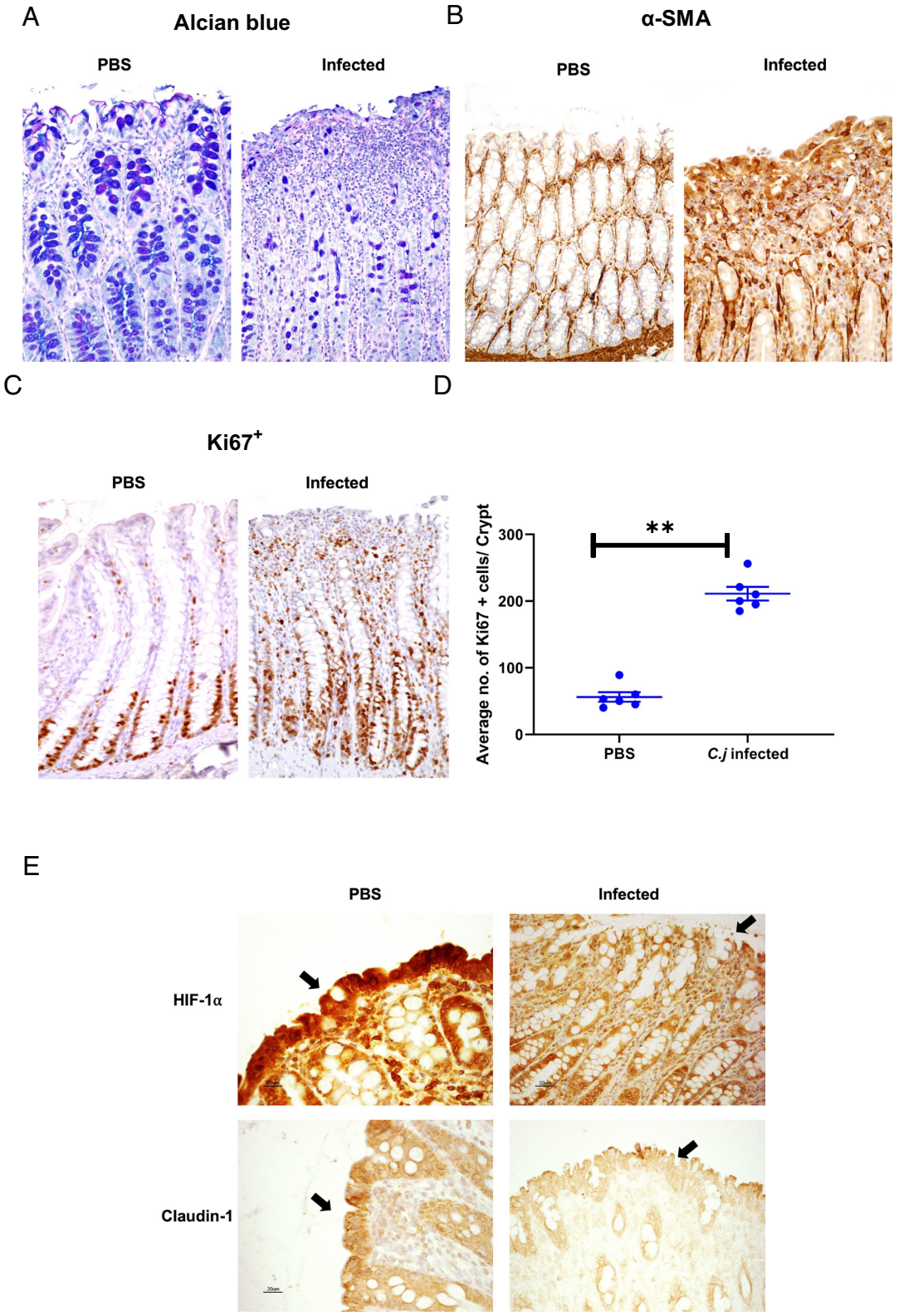

Fig. 2. *C. jejuni* induced pathophysiological changes of colonic tissue during acute stage. (*A*) Representative image of Alcian blue staining for goblet cells of colonic tissue day 3 post infection. Original magnification, 40X. (*B*) Representative IHC image of day 3 post infection colonic tissue with α-Smooth Muscle Actin (SMA) specific antibody (to view tissue repair). (*C*) Representative image of Ki67+ proliferated cell localization and (*D*) count of Ki67+ cells/crypts in colonic tissue day 3 post infection. (*E*) Representative IHC image of day 3 post infection colonic tissue with HIF-1α and Claudin-1 specific antibody. Original magnification, 40X. All error bars show ± SD. Statistical analysis was done by unpaired two-tailed *t* test. $*P < 0.05$; $**P < 0.01$; $***P < 0.001$; $****P < 0.000$.

in normal colon epithelial cells due to the typical hypoxic environment of the gut, as previously studied (7, 19, 20, 22). We performed IHC staining with anti-HIF-1α antibody from day 3 colon samples of both infected and uninfected animals. HIF-1α levels in colon sections from the infected group were lower than in those from mock-infected animals (Fig. 2*E*), indicating a less hypoxic environment in the *C. jejuni*-infected animals, and suggesting epithelial oxygenation is increased during the acute stage of *C. jejuni* infection in the ferret. The tight junction protein claudin-1 is positively regulated by HIF-1α (19), so we also analyzed tissue with anti-claudin 1 antibody. Consistent with the decreased level of HIF-1α in animals infected with *C. jejuni*, claudin 1 protein levels were also decreased in these animals compared to what we observed in mock-infected controls (Fig. 2*E*). Loss of claudin-1 and subsequent disruption of tight junction integrity may play a role in the dissemination of *C. jejuni* in the ferret.

Effects of *C. jejuni* Infection on Microbiota and Metabolites in the Ferret Colon. The microbial composition in the colon contents of these 5- to 6-wk-old ferrets is made up predominantly of *Clostridia* sp., as determined by 16S rRNA gene sequencing (Fig. 3*A*). Dysbiosis and depletion of *Clostridium* after streptomycin treatment enables *Salmonella* Typhimurium to colonize the murine gut (23). Our data suggest that, in contrast, there is no negative effect of *Clostridium* on *C. jejuni* colonization in the ferret gut (23). Infected ferrets do not have a significantly altered overall microbiota (PERMANOVA, R2 = 0.129, Pr(>F) = 0.097) (*SI Appendix*, Fig. S3*A*), consistent with microbiota analysis of *C. jejuni*-infected humans (24). The low microbial diversity in the guts of 5- to 6-wk-old ferrets may help explain their susceptibility to *C. jejuni* infection.

By performing differential abundance analysis (DESeq2) of zero-radius operational taxonomic units (ZOTUs), we could identify differentially abundant taxa in colonic contents of the infected group from day 3 after infection. We observed elevated abundances of *Clostridium* sensu stricto 1 (ZOTU13), and (as expected) *Campylobacter* (ZOTU6) (log2 fold change = 25.13, *P*-adj = 4.85e-16). This is reminiscent of *C. rodentium* infection in mice, which also resulted in greater *Clostridia* abundance (9). We also observed decreased abundance of *Enterococcus durans* (ZOTU12) (log2 fold change = −9.53, *P*-adj = 5.40e-05) (Fig. 3*B*). *Enterococcus durans* sp1 exhibits antiinflammatory effects and reduced signs of DSS-induced colitis in mice (25), suggesting perhaps that the reduced level of *E. durans* ZOTU12 abundance may contribute to the induction of gastroenteritis in ferrets.

Metabolites such as L-lactate, aspartate, malate, formic acid, and others, which may be derived from the host or the microbiota, regulate growth and expression of virulence factors in various pathogenic bacteria (26–28). Less is understood about how gut metabolites influence *C. jejuni* growth during inflammation. One study determined that L-fucose, a component of mucin, induces *C. jejuni* growth and regulates colonization in a piglet model (29). Our histopathological analysis found that surface localized colonocytes were present after *C. jejuni*-induced colonic hyperplasia, which may influence the gut metabolites present during infection. To identify host-derived metabolites that might support *C. jejuni* growth during infection, we collected colon contents from uninfected and infected animals at 72 h postinfection and subjected them to targeted mass spectrometry. Principal component analysis indicated significant difference in gut metabolite profiles between infected and mock-infected groups (Fig. 3*C*). Of those metabolites found to be differently abundant, we focused on different known potential carbon sources for *C. jejuni*.

Carbon sources that enable *C. jejuni* growth during infection are undefined. L-fucose is one of these, and the fucose transporter (*fucP*) is essential for colonization in a piglet model, although the fucose-utilizing genes are not widely distributed among different strains (29). Studies carried out in vitro revealed that *C. jejuni* can use TCA cycle intermediates such as citrate, malate, α-ketoglutarate, and fumarate as carbon sources, and lactate use has also been reported (5, 30). We observed lactate levels elevated nearly 10-fold in colon contents of *C. jejuni*-infected ferrets while TCA cycle intermediates citrate, malate, and alpha ketoglutarate levels were significantly lower in samples from the infected group compared with those from the uninfected group (Fig. 3*D*). Host-derived lactate serves as a sole nutrient source for several pathogens, and lactate-utilizing genes are also essential for disease progression of *Salmonella* Typhimurium, *Neisseria* species, and *H. influenzae* (26, 31, 32). Furthermore, short-chain fatty acids derived by the microbiota, especially butyrate and propionate, reduce enteric colonization of pathogens such as *Salmonella* Typhimurium and influence the inflammatory response in gut (23). Butyrate levels in colonic contents from infected ferrets were significantly higher than from the PBS control group, while other short-chain fatty acid such as propionate and acetate were not significantly changed (Fig. 3*E*). Butyrate induces expression of the BumSR regulon, products of which are essential for commensal colonization of *C. jejuni* in the day-of-hatch chicken and in humans (33). Based on the metabolite study, we sought to determine whether elevated lactate and butyrate in colonic contents of infected ferret could influence the growth of *C. jejuni* during inflammation.

The Lactate Permease (*lctP*) Operon Is Essential for *C. jejuni* Expansion during Ferret Infection. We tested *C. jejuni* growth in mucin-containing minimal media supplemented with either 10 mM butyrate or 10 mM L-lactate and observed better growth with L-lactate in the media than with butyrate (Fig. 4*A*). The genome of *C. jejuni* 11168 wild-type contains four genes in an apparent operon *cj0076c-0075c-0074c-0073c*, where *cj0076c* encodes a lactate transporter (*lctP*) and *cj0075c-cj0074c-cj0073c* encode a nonflavin iron–sulfur-containing three subunit membrane oxidoreductase which convert L-lactate to pyruvate. This operon is essential for L-lactate utilization in vitro (34). We hypothesized that lactate and *lctP* would be essential for growth during infection when lactate levels are elevated.

We constructed a mutation of *lctP* (*lctP::kan*) using a polar kanamycin-resistance cassette to knock down expression of the entire operon. RT-PCR of the wild-type locus using primers specific for the junctions between the open reading frames confirmed these genes are cotranscribed and that no detectable transcription of *cj0075c-cj0074c-cj0073c* is observed in the *lctP::kan* strain (*SI Appendix*, Fig. S4*A*). To complement this mutant, we amplified the entire operon and inserted it into the *lctP::kan* strain between the 16S rRNA and 23S rRNA genes using the prRNA-Hygro^R suicide vector (35). We measured the growth of wild-type, *lctP::kan*, and the complemented *lctP::kan* strain in media containing 10 mM L-lactate. The wild type and complemented *lctP::kan* strains grew similarly, whereas the *lctP::kan* mutant strain showed a significant growth defect achieving peak growth nearly 100-fold less than that of wild-type and complemented strains (Fig. 4*B*). Media in which wild type or *lctP::kan/C* were cultured retained low L-lactate while media in which the *lctP::kan* strain was cultured retained levels similar to the sterile culture medium. These data confirm that the *lctP* locus contributes to L-lactate uptake (*SI Appendix*, Fig. S4*B*).

To examine whether lactate use is required by *C. jejuni* during infection, we infected ferrets with either wild-type *C. jejuni* or the *lctP::kan* mutant and measured fecal bacterial loads at 24- and 72-h postinfection and then in the colon of animals euthanized 72 h post-infection, per Michigan State University IACUC guidelines. Fecal loads of wild-type and the *lctP::kan* were equivalent after 24 h, but by 72 h, wild-type *C. jejuni* was two orders of magnitude higher than the *lctP::kan* mutant (Fig. 4*C*). Similarly, wild-type *C. jejuni* colonized the colonic tissue three orders of magnitude greater than the *lctP::kan* strain at 72 h (Fig. 4*D*). Supporting this result, immunohistochemistry demonstrated a higher number of adherent wild-type cells associated with the colonic epithelium with some cells colonizing deep into the colonic crypts. In contrast, very few *lctP::kan* cells were observed associated with the epithelial surface and they did not colonize within the crypts, remaining predominantly associated with the mucus (Fig. 4*E*). In response to reduced infection, we also observed a diminished inflammatory score in colon tissue from *lctP::kan*-infected animals when compared to that of wild-type infected animals (although it was significantly higher than the PBS control group) (Fig. 4*F*). Overall, our

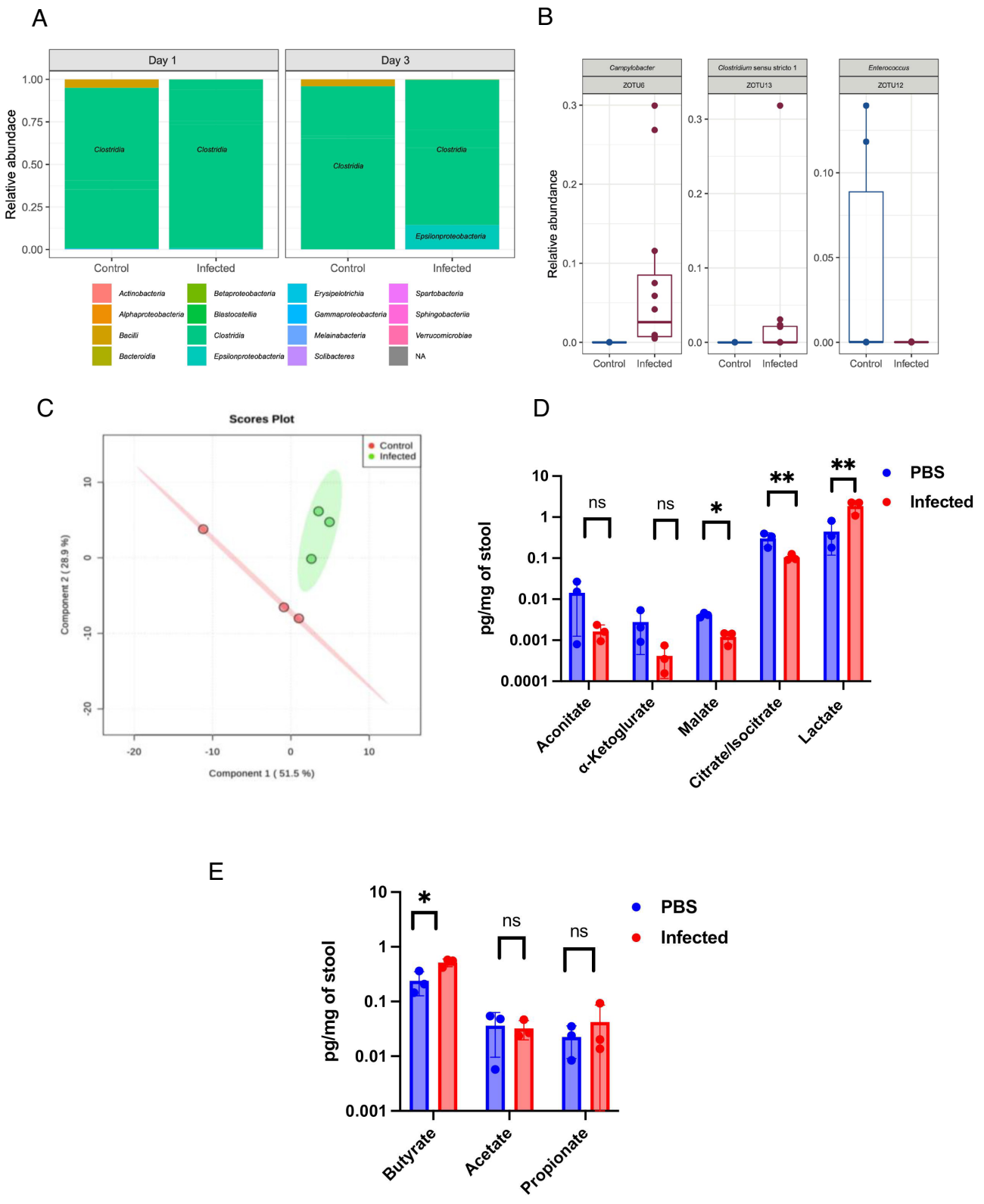

Fig. 3. Changes of gut microbiota and metabolites after infection with *C. jejuni* in ferret. (*A*) Microbial representation at class-level, based on 16 s RNA sequencing, in cecal contents of infected and uninfected (PBS) ferrets day 1 and day 3 post infection. Color coding for classes is shown below the chart. (*B*) Differentially abundant taxa were found on day 3 between infected and uninfected (PBS) ferrets using DESeq2. As expected, *Campylobacter* (ZOTU6) and *Clostridium* sensu stricto 1 (ZOTU13) members were significantly enriched in the infected group compared to the uninfected control group (log2 fold change = 8.93, *P*-adj = 2.55e-06 and log2 fold change = 25.13, *P*-adj = 4.85e-16, respectively). On the other hand, *Enterococcus durans* (ZOTU12) was the only one significantly decreased in the infection group (log2 fold change = −9.53, *P*-adj = 5.40e-05). (*C*) Difference of overall metabolites of colon contents between infected and uninfected control animals on day 3 post infection by principal component analysis (PLSDA model). Each circle indicated overall metabolites of each animal, $n = 3$. Concentrations of selected metabolites of colon contents from infected and uninfected animals on day 3, such as (*D*) different TCA cycles intermediates and (*E*) short chain fatty acids, were determined by LC–MS mass spectrometry ($n = 3$). Error bars represent SD. Statistical analysis was done by unpaired two-tailed *t* test. **P* < 0.05; ***P* < 0.01; ****P* < 0.001; *****P* < 0.000.

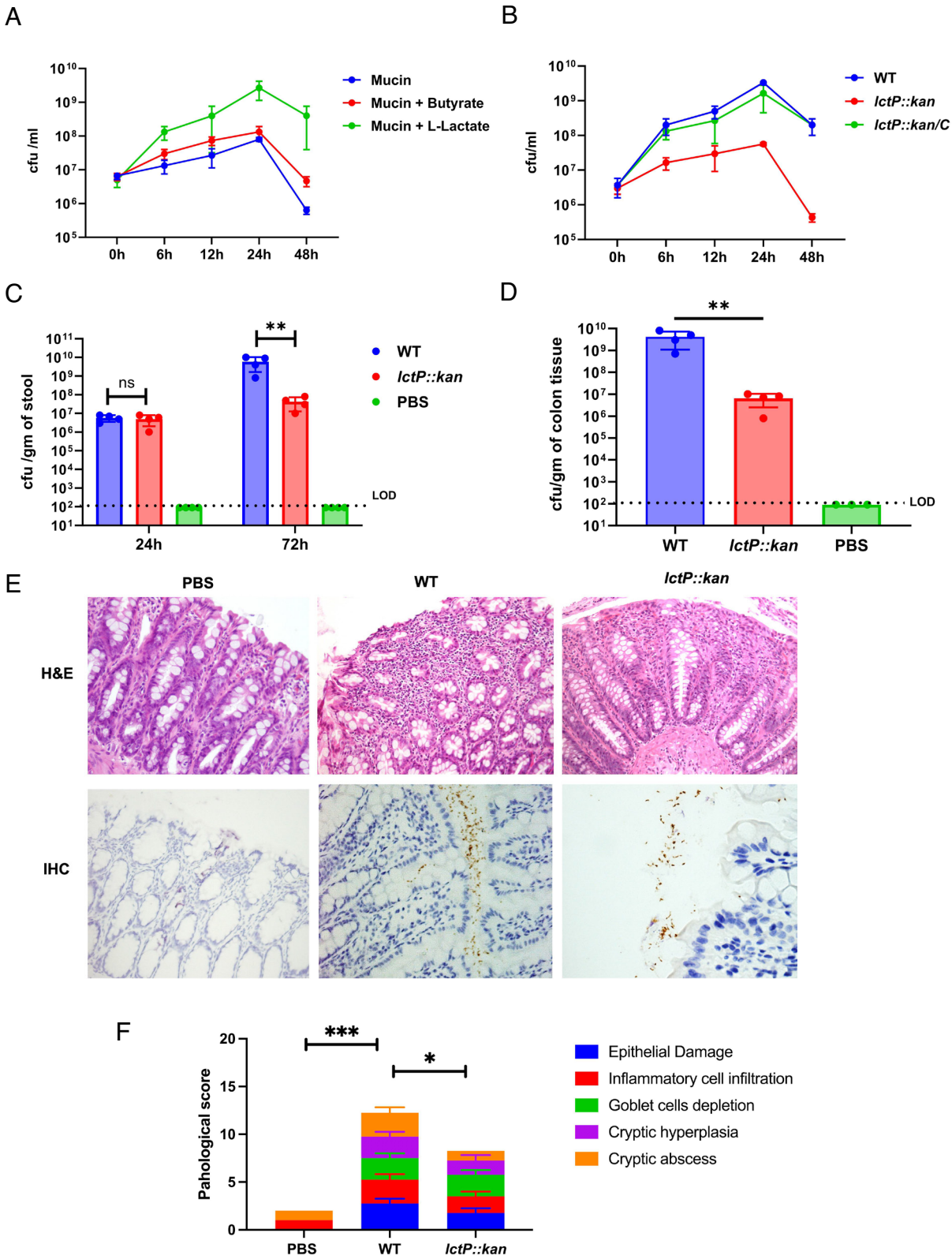

Fig. 4. *lctP* operon is essential for pathogenesis of *C. jejuni* in Ferret. (*A*) Growth of C. *jejuni* 11168 WT strain in minimal media containing mucin with and without butyrate (10 mM) and L-lactate (10 mM) over 48 h was determined by CFU counts (n = 3). (*B*) WT, *lctP::kan* and complementary *lctP::kan/C* strains were grown in minimal media containing mucin with L-lactate (10 mM); cfu/mL growth was determined over 48 h (n = 3). Bacterial comparative colonization was determined in 5- to 6-wk old ferrets infected orally with either wild type or *lctP::kan* (dose of 10^9 CFU/mL). Bacterial loads in (*C*) stool and (*D*) colonic tissue were determined by CFU counts at different time intervals. (PBS n = 3 and infected group n = 4). (*E*) Representative images of H&E stained day 3 colonic tissue (20X) and IHC with day 3 colonic tissue using *C. jejuni* specific antibody (40X) (n = 3). (*F*) Histological scores of colonic tissue (PBS, WT and *lctP::kan* groups) were determined on day 3 post infection (PBS n = 3, Infected n = 4). LOD indicates the limit of detection. Error bars represent SD. Statistical analysis was done by one-way AONOVA. *P < 0.05; **P < 0.01; ***P < 0.001; ****P < 0.000.

ferret data suggest that the *lctP* operon is not essential for colonization by *C. jejuni* but is required for bacterial growth within the colon after colonization.

C. jejuni is a commensal microbe of chickens and establishes high loads after infection with limited inflammation that is not sufficient to clear the infection (5). Lactate is found in varying concentrations throughout the chicken gastrointestinal tract, typically decreasing as it progresses from the upper intestine to the lower intestine and ceca. Notably, in 7-d-old chickens, the average lactate concentration in the ceca is 4.2 ± 2.9 mmol/kg (36). We carried out competitive colonization assays between wild-type *C. jejuni* 11168 and the *lctP::kan* derivative in day-of-hatch chicks to assess whether lactate is a critical growth substrated for *C. jejuni*. Strains were mixed at a 1:1 concentration and inoculated into day-of-hatch chicks by oral gavage. We harvested cecal contents on day 7 postinfection and determined the competitive index for each strain by measuring the number of kanamycin-resistant (*lctP::kan* mutant) and kanamycin-sensitive (wild-type) bacteria. There was no competitive disadvantage for the *lctP* mutant strain in chicks (*SI Appendix*, Fig. S5*B*), indicating that despite its availability, lactate uptake and utilization does not contribute to commensal colonization of chicks by *C. jejuni*.

The *lctP* Operon Is Required for Adherence and Invasion of Human Colonocytes. Metabolism of proliferating cells, such as the Ki67+ cells that are significantly elevated in infected ferrets, results in lactate production, which is the likely source of the elevated lactate we observe in infected animals. Similarly, human cancers have been found to produce and secrete lactate from metabolism of glucose, which has been termed the "Warburg effect" (21). To investigate whether host-derived lactate influences *lctP* expression, we introduced a plasmid containing a *lctP-gfp* promoter fusion into *C. jejuni* and infected HCT116 cells, a human colon carcinoma cell line. GFP levels were three-fold higher when bacteria were cultured with HCT116 cells compared to cultures lacking the HCT116 cells (Fig. 5*A*). These data suggest that host-derived lactate produced by HCT116 cells induces expression of *lctP*.

Because the *lctP* operon is needed for *C.jejuni* growth in the ferret colon, we explored the role of the *lctP* operon further by infecting HCT116 cells with either wild-type, *lctP::kan*, or the *lctP::kan* mutant. After 1 h of infection, we observed a small but statistically significant decrease in both adherence and invasion of the *lctP::kan* mutant when compared to wild type and the complemented mutant (Fig. 5*B*). This is consistent with what was observed for the wild type and mutant during ferret infection, although the magnitude of the mutant defect during infection was greater than what we observe with cultured cells. To measure how the *lctP* operon contributes to lactate use from the host, we analyzed extracellular lactate levels in the culture media and intracellular lactate levels in cells after infection of the HCT116 cell line. Infection with either the wild type or complemented *lctP::kan* strain resulted in lower lactate levels in culture media after 1 h of infection, whereas we observed no significant change in lactate levels in the medium of cells cultured with the *lctP::kan* mutant. Similarly, we observed decreased intracellular lactate levels in cells infected with wild type and the complemented mutant, but not the *lctP::kan* mutant (Fig. 5 *C* and *D*). We conclude that *C. jejuni* uses the LctP pathway for lactate uptake when extracellularly and intracellularly associated with host cells.

To further explore the role of lactate during *C. jejuni* infection of colonocytes, we treated HCT116 cells with two inhibitors i) sodium oxamate, a competitive inhibitor of lactate dehydrogenase, and ii) 2-deoxyglucose, a noncompetitive hexokinase inhibitor that reduces lactate production by inhibiting the glycolysis pathway (37, 38). Both inhibitors were confirmed to significantly reduce lactate levels when compared to untreated cells, without reducing cell viability (Fig. 5*E*). We then infected treated and untreated cells with wild-type *C. jejuni* and measured bacterial adherence and invasion. We observed a slight, but statistically significant reduction in *C. jejuni* adherence and invasion in both treated groups when compared to the untreated controls (Fig. 5*F*). These results suggest that host-derived lactate contributes to bacterial growth during adherence and invasion of *C. jejuni* to human colonocytes.

LctR Is a Potential Regulator of the *lctP* Operon. Our data indicate that LctP-dependent lactate utilization promotes *C. jejuni* growth during infection, raising the question of whether *lctP* expression itself is regulated during infection. An earlier study examining transcriptome dynamics of *C. jejuni* demonstrated a reduction in *lctP* operon transcripts of over five-fold in cells undergoing transition from high (7.5%) to low (1.88%) oxygen levels (39). We used RT-qPCR to evaluate the expression of the *lctP* operon following a 2-h incubation in mucin media containing lactate, conducted under both anaerobic and microaerobic conditions. Expression of *lctP* was reduced two- to threefold in the oxygen-limited condition when compared to the microaerobic condition (Fig. 6*A*). These data suggest that *lctP* expression is influenced by environmental oxygen levels.

In other bacterial pathogens, *lctP* is regulated by oxygen and the ArcAB two-component system, which *C. jejuni* lacks (32, 40). During anaerobic growth of these microbes, the response regulator ArcA is phosphorylated by the sensor kinase, ArcB, and phosphorylated ArcA binds to the *lctP* promoter, repressing its expression. A redox-sensitive regulator in the related *Helicobacter pylori* is HP1021, which represses transcription of different genes such *gluP* and *fecA3* (among others) during growth in low oxygen (41). A homologous gene of *C. jejuni*, *cj1608*, encodes a product that binds to the *oriC* promoter via a high-affinity consensus binding site (5′-TGTTACA-3′) repressing replication of *C. jejuni* (a similar phenotype has been observed in *H. pylori*) (42). Two copies of this palindromic sequence are present upstream of the *C. jejuni lctP* operon at position −25 to −85 relative to the transcription start site, which would place binding by CJ1608 within the potential RNA polymerase binding site (Fig. 6*B*). Based on data presented in the next section, we propose naming CJ1608 "*Lct*P ***R***egulator" (LctR).

We expressed and purified histidine-tagged LctR and used it in electrophoretic mobility shift assays with FAM-labeled p_{lctP}. Increasing amounts of 6xHis-LctR gradually reduced the mobility of labeled $p_{lctP,}$ which was not observed for the nonspecific binding control, a FAM-labeled region of the *mapA* gene (43) (Fig. 6*C*). From this, we concluded that 6xHis-CJ1608 specifically binds to p_{lctP}.

Structural modeling of LctR with AlphaFold 2 indicated distinct N-terminal and C-terminal domains (41, 44, 45). The C-terminal domain includes a helix-turn-helix (HTH) motif (Fig. 6*D*) common to DNA binding proteins, while the N-terminal domain includes three surface-exposed cysteine residues (Cys-27, Cys-165, and Cys-233; Fig. 6*D*). The *H. pylori* HP1021 protein contains six cysteine residues, at least some of which control conformational changes of the protein in response to oxidation levels (41). Aligning sequences of HP1021 and LctR found that residue Cys-27 is conserved in the two proteins (*SI Appendix*, Fig. S6).

Because our predicted model of LctR includes surface-exposed cysteines, we hypothesized that the protein may form cysteine-mediated oligomers, which may contribute to redox-sensitive changes in disulfide bond formation that could play a role in its activity. Size exclusion chromatography suggests that LctR exists as dimer in solution, with a molecular weight of 80 kDa (Fig. 6*E*). Air-oxidized LctR migrates on nonreducing SDS-PAGE as multiple

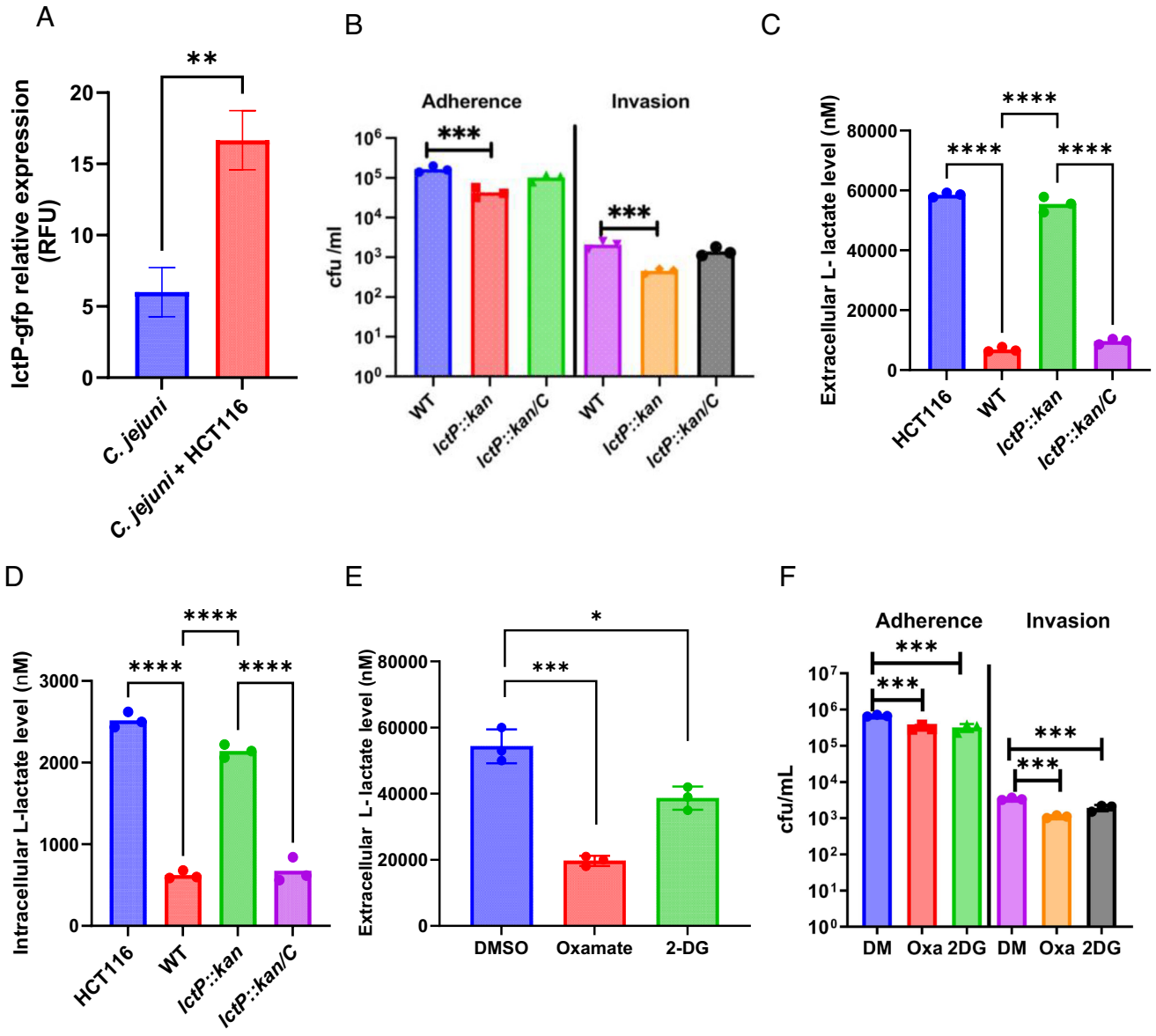

Fig. 5. Host-derived lactate influences the adherence and invasion of *C. jejuni* in vitro: (*A*) Relative fluorescence units (RFU) of *C. jejuni* type strain carrying *lctP-gfp* fusion plasmid were measured with or without HCT116 cells after 1 h of infection by spectrophometer. (n = 3). Statistical analysis was done by unpaired two-tailed t test. (*B*) Adherence and invasion ability of WT, *lctP::kan* and *lctP::kan/C* was determined after of 1 h of infection in HCT116 cells at an MOI was 10 (n = 3). (*C*) Extracellular and (*D*) intracellular L-lactate levels in HCT116 cells were determined after 1 h of infection with WT, *lctP::kan* and *lctP::kan/C* by ELISA (n = 3). (*E*) Extracellular lactate level was determined after treatment with sodium oxamate (30 mM) and 2-deoxy glucose (1 mM) by ELISA (n = 3). (*F*) Adherence and invasion of WT was determined in sodium oxamate and 2-deoxyglucose and untreated HCT116 cells after 1 h of infection (n = 3). Error bars represent SD. Statistical analysis was done by one-way AONOVA. *P < 0.05; **P < 0.01; ***P < 0.001; ****P < 0.000.

species, predominantly as a monomer but with evidence of dimer and even multimer formation (Fig. 6*F*). The protein forms a dimer in prolonged storage conditions, as observed with gel filtration (Fig. 6*F*). Incubating the protein with the reducing agent 10 mM DTT, we observed only a single species that migrates on nondenaturing SDS-PAGE consistent with its being a monomer, indicating that dimers and multimers are a consequence of thiol-oxidation. To further explore the impact of reducing or oxidizing LctR on its DNA binding ability, we tested four concentrations of LctR (50, 100, 150, and 200 nM), both air-oxidized after 30 min treatment with DTT (10 mM). After exposure to the reducing agent, LctR binding to p_{lctP} was observed at lower concentrations of protein LctR (50 and 100 nM) than that observed for oxidized LctR (Fig. 6*G*). Based on these results, we conclude that reduced LctR remains in a more stable, likely monomeric, conformation favored for DNA binding. Given the location of the putative LctR binding site in the *lctP* promoter, we suggest that LctR represses expression of the lactate utilization genes when bound in its reduced, monomeric form.

Discussion

C. jejuni colonization results in different outcomes depending on the host: a commensal state, which occurs in the avian gut and results in little inflammation, and a pathogenic state in humans that leads to the development of intestinal inflammation and diarrheal disease (5). Because of these differences, the day-of-hatch chicken is a valuable natural host model for understanding molecular mechanisms of commensal colonization of *C. jejuni* in the avian gut but is unsuitable for gathering information about the disease state (5). In contrast, the weaning-aged ferret develops a self-limiting infection and intestinal disease similar to humans. Due to these similarities, we examined the changes to the intestinal environment during

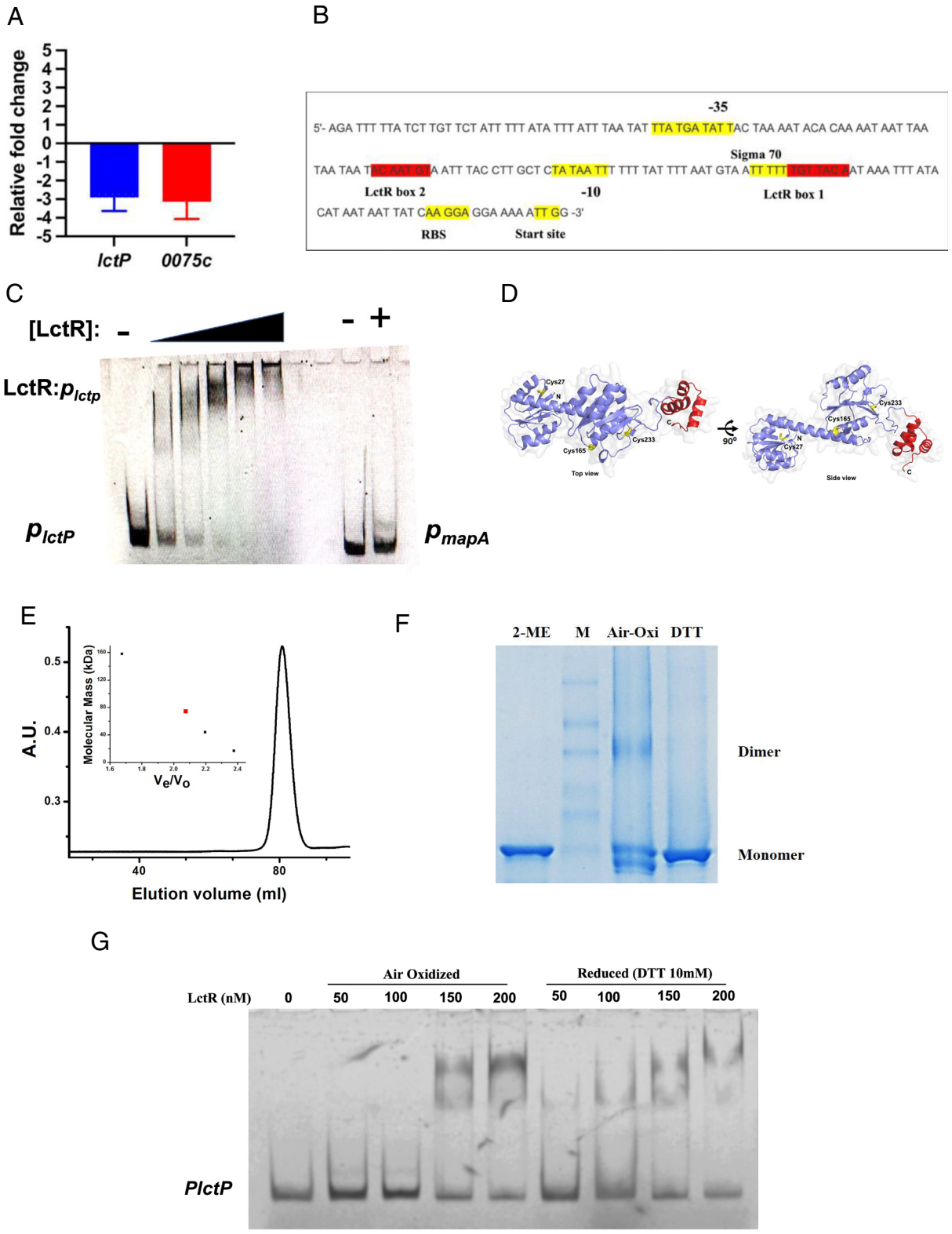

Fig. 6. Redox switch protein LctR binds to the promoter of *lctP*. (*A*) Transcription analysis of two *lctP* operon genes (*lctP* and *0075c*) at 2 h after growth of WT strain in minimal media containing mucin with lactate (10 mM) by quantitative RT-PCR in anaerobic and microaerobic condition. Changes in gene expression of WT strain in anaerobic conditions compared with microaerobic conditions were determined by the $2^{-\Delta\Delta CT}$ method. Data are represented as the mean value from three independent experiments ± SD. (*B*) Predicted promoter region of LctP (with important regions, such as −35, −10, and RBS, highlighted in yellow) and two probable LctR binding consensus sequences (5′-TGTTACA-3′, highlighted in red). (*C*) Determination of purified 6 × His-LctR binding capacity to the promoter region of *lctP* (P_{lctP}) by EMSA. Increasing amounts of purified 6 × His-LctR were added to binding reaction mixtures containing approximately 0.25 nM either P_{lctP} promoter fragment or the *mapA-ctsW* (P_{mapA}) intergenic region as a nonspecific control. Results are representative of three biological replicates. (*D*) A predicted structure of LctR by alphafold program. Three cysteine residues are highlighted in yellow and a predicted HTH domain is highlighted in red. (*E*) Size exclusion chromatography of purified LctR. LctR eluted from Superdex column showed dimer form in normal condition. (*F*) The thiol based redox state of LctR was analyzed by incubating with oxidizing (Air oxidation) and reducing (DTT) agent. Redox state of LctR was determined by 10% SDS page in nonreducing condition and Coomassie staining. Representative image of three biological replicates. (*G*) Determination of LctR binding capacity to the *PlctP* promoter fragment in oxidized (Air oxidized) and reduced (DTT treated) condition by EMSA. Representative image of three biological replicates.

C. jejuni infection of ferrets to identify strategies the bacterium uses to support growth during acute infection.

We observed that *C. jejuni* infection led to moderate to severe gastroenteritis signs in ferrets. After infecting with 10^9 bacteria, we observed that the *C. jejuni* population grew within 2 to 3 d, which was accompanied by cryptic hyperplasia and the accumulation of undifferentiated cells on the colon surface. During infection, we also observed instability of HIF-1α in colonocytes, which may indicate increased epithelial oxygenation. We detected no significant changes in the microbiota during *C. jejuni*-induced inflammation although we did detect elevated lactate, which we hypothesized to be a carbon source for *C. jejuni* growth during infection.

During gut homeostatic conditions, microbiota-derived short-chain fatty acids, especially butyrate, induce peroxisome proliferator–activated receptor γ (PPAR-γ) signaling in mature differentiated epithelial cells to maintain a state of physiological hypoxia in the lumen through oxygen consumption via β-oxidation (46, 47). Decreased oxygen availability in epithelial cells stabilizes HIF-1α which controls tight junction proteins, mucus production, and antimicrobial peptides (48). The base of intestinal crypts is more oxygenated than the lumen because of the presence of undifferentiated amplifying epithelial cells which use anaerobic glycolysis and therefore consume less oxygen (21, 47, 49). The *Enterobacteriaceae* family of facultative anaerobic bacteria adopt different strategies to alter gut homoeostatic conditions for expansion in the gut (46, 47, 49). For example, *Salmonella* Typhimurium infection triggers neutrophil infiltration in the gut lumen, which causes depletion of *Clostridia* thereby increasing oxygen levels by altering the metabolism of mature colonocytes (46). *Salmonella* Typhimurium then also utilizes oxygen as an electron acceptor and lactate as a carbon source to grow in the gut lumen (40). In contrast, *Citrobacter rodentium* causes colon cryptic hyperplasia in mice through its type III secretion system (T3SS) which increases epithelial oxygenation by recruiting immature colonocytes (which lack β-oxidation metabolism) to the surface of the colon (46). During growth of *C. jejuni* in the ferret, we observed infiltration of neutrophils in infected colonic tissue, and prominence of *Clostridia* species and the metabolite butyrate which is quite different FROM *S. typhimurium* infection in mice (49). We hypothesize that the strategy of *C. jejuni* expansion in ferrets during infection is more like *C. rodentium* in mice.

The obligate microaerophile *C. jejuni* requires low levels of oxygen [a partial oxygen tension (pO_2) of 2 to 10%] for growth (50). Oxygen is an electron acceptor for ATP production, growth, and motility of *C. jejuni* (50). We hypothesize that accumulation of undifferentiated immature colonic cells on the colonic surface during *C. jejuni* infection increases epithelial oxygenation. During inflammatory response to pathogens in the gut, epithelial oxygenation increases between 3 to 10% which indicates a microaerobic condition is created near epithelial cells (46, 47). This would create an appropriate environment for *C. jejuni* microaerobic respiration and growth in the gut (51). While the T3SS and its effectors in *Citrobacter rodentium* induce recruitment of proliferative undifferentiated epithelial cells during infection in mice, in the case of *C. jejuni,* the factors that induce colonic cell proliferation are not clear. *C. jejuni* secretes effector proteins, called Campylobacter invasion antigens (Cia), through a flagellum-associated mechanism, triggering signal transduction in host cells (9, 52–54). Bile salts induce the synthesis of Cia proteins, and we detected elevated levels of primary bile salts and decreased the level of one secondary bile salt, taurolithocholic acid (TLCA), which has an antiinflammatory effect on LPS-induced macrophages, during the acute stage of infection (55, 56). We hypothesize that during infection, elevated bile salts induce Cia proteins, leading to proliferating cells in the colon, which aids the growth of *C. jejuni*.

Nutrient resources, especially carbon sources, that support *C. jejuni* expansion in the inflamed gut are not well known. L-fucose is the only carbohydrate reported that induces growth and colonization (analyzed in a piglet model). Genes for catabolism of L-fucose are not well conserved among *C. jejuni* isolates from different sources (57). *C. jejuni* can metabolize some organic acids like citrate, butyrate, succinate, and lactate (58). Our targeted metabolite study found elevated lactate levels in colon contents; given that host-derived L-lactate can serve as a major carbon source for *Salmonella* Typhimurium in a mouse model (40), we explored lactate as a potential growth substrate for *C. jejuni.* That the *C. jejuni lctP* operon mutant exhibited a colonization defect (day 3) led us to conclude that lactate is a carbon source for *C. jejuni* during infection. Supporting this, the *lctP* locus (0076c-0073c) is present in 2,138 out of the 2,140 strains we queried from public collections such as *the Campylobacter* pubMLST website (http://pubmlst.org/campylobacter/), most of which were isolated from human patients (Dataset S1). We did not focus on identifying the potential sources of elevated lactate levels in the gut (host- or microbiota-derived); however, we observed an accumulation of undifferentiated colonocytes, which produce lactate from glucose on the surface of the colon. In addition, we did not observe drastic changes in the microbiota that might account for new sources of lactate. Elevated lactate levels were similarly observed in *C. rodentium* infection of mice with the presence of undifferentiated colonocytes. Based on these data, we hypothesize that elevated L-lactate in the ferret gut is also host-derived (59). Adherence and invasion of colorectal cancer epithelial cells (HCT116) by *C. jejuni* was reduced in the presence of two lactate inhibitors, sodium oxamate (LDH inhibitor), and 2-deoxyglucose (hexokinase inhibitor), suggesting that these traits, along with growth in vivo, are influenced by lactate levels. We concluded that host-derived lactate influences *C. jejuni* adherence and invasion.

In some pathogenic bacteria, thiol-based regulators play a vital role in responding to cellular stressors, including oxidative stresses, the production of virulence factors, and colonization (60, 61). In our study, we identified a potential thiol-based redox orphan regulator that we named LctR. This regulator bears similarity to an *H. pylori* redox regulator encoded by HP1021 that represses differential gene expression under anaerobic conditions (41). Our in vitro experiments suggest that expression of the *lctP* gene in *C. jejuni* relies on oxygen availability. Furthermore, we observed that the oxidized, dimeric form of LctR has reduced promoter binding capacity at the putative RNA polymerase binding site, compared to its reduced, monomeric form, which suggests a redox-dependent impact on transcription activation of *lctP*. Consequently, we hypothesize that reduced LctR represses *lctP* expression, such as under conditions of low oxygen availability. Our in vivo work demonstrates that expression of the *C. jejuni lctP* operon is crucial during the inflammatory stage, coinciding with evidence of rising epithelial oxygen levels in the gut. This observation allows us to draw a connection between the regulation of *lctP* by LctR, as demonstrated in our in vitro and in vivo study.

In conclusion, our findings provide a deeper understanding of how the host response to *C. jejuni* infection appears to contribute to growth of the microbe during infection.

Materials and Methods

Materials and Methods describing the bacterial growth conditions, *C. jejuni* mutant and complementation construction, ferret infection and colonization assay, histology, immunohistochemistry, 16 RNA sequencing, metabolites extraction and liquid chromatography-mass spectrometry analysis, quantitative real time PCR, adherence and invasion assay within human intestinal epithelial cells, *lctP* GFP expression assay, measurement of extracellular and

intracellular lactate level within intestinal epithelial cells, protein expression and purification, thiol redox state of LctR in vitro assay, EMSA, and size exclusion chromatography are described in detail in *SI Appendix*. All bacterial strains, plasmids constructed, and primers used in this work are included in *SI Appendix*, Table S1 and S2, respectively. The animal experiment protocol has been reviewed and approved by Michigan State University Institutional Animal Care and Use Committee (IACUC).

Data, Materials, and Software Availability. All study data are available in Github (62). Other data are included in the article and/or supporting information.

ACKNOWLEDGMENTS. This work was supported in part by NIH award AI111192 and the Michigan State Rudolph Hugh Endowment (to V.J.D.) and AI166535 (to J.G.J.). S.C. was supported by NIH award CHE2203472 and NIH award GM128959 (to R.P. Hausinger and J. Hu), N.S. was supported by the Michigan State University Plant Resilience Institute. S.M.C. was a trainee of the SEC Emerging Scholars Program.

Author affiliations: [a]Department of Microbiology, Genetics, & Immunology, Michigan State University, East Lansing, MI 48824; [b]Department of Microbiology, University of Tennessee, Knoxville, TN 37996; and [c]Department of Pathobiology and Diagnostic Investigation, Michigan State University, East Lansing, MI 48824

1. M. E. Patrick *et al.*, Features of illnesses caused by five species of *Campylobacter*, Foodborne Diseases Active Surveillance Network (FoodNet)–2010–2015. *Epidemiol. Infect.* **146**, 1–10 (2018).
2. E. Tacconelli *et al.*, Discovery, research, and development of new antibiotics: the WHO priority list of antibiotic-resistant bacteria and tuberculosis. *Lancet Infect. Dis.* **18**, 318–327 (2018).
3. R. Manfredi, A. Nanetti, M. Ferri, F. Chiodo, Fatal *Campylobacter jejuni* bacteraemia in patients with AIDS. *J. Med. Microbiol.* **48**, 601–603 (1999).
4. C. Fitzgerald, Campylobacter. *Clin. Lab. Med.* **35**, 289–298 (2015).
5. K. T. Young, L. M. Davis, V. J. Dirita, *Campylobacter jejuni*: Molecular biology and pathogenesis. *Nat. Rev. Microbiol.* **5**, 665–679 (2007).
6. C. Lupp *et al.*, Host-mediated inflammation disrupts the intestinal microbiota and promotes the overgrowth of *Enterobacteriaceae*. *Cell Host Microbe* **2**, 204 (2007).
7. J.-Y. Tinevez *et al.*, Shigella-mediated oxygen depletion is essential for intestinal mucosa colonization. *Nat. Microbiol.* **4**, 2001–2009 (2019).
8. F. Rivera-Chávez, J. J. Mekalanos, Cholera toxin promotes pathogen acquisition of host-derived nutrients. *Nature* **572**, 244–248 (2019).
9. C. A. Lopez *et al.*, Virulence factors enhance *Citrobacter rodentium* expansion through aerobic respiration. *Science* **353**, 1249–1253 (2016).
10. K. W. Nemelka *et al.*, Immune response to and histopathology of *Campylobacter jejuni* infection in ferrets (*Mustela putorius* furo). *Comp. Med.* **59**, 363–371 (2009).
11. R. O. Watson, V. Novik, D. Hofreuter, M. Lara-Tejero, J. E. Galán, A MyD88-deficient mouse model reveals a role for Nramp1 in *Campylobacter jejuni* infection. *Infect. Immun.* **75**, 1994–2003 (2007).
12. M. Stahl *et al.*, A novel mouse model of *Campylobacter jejuni* gastroenteritis reveals key pro-inflammatory and tissue protective roles for Toll-like receptor signaling during infection. *PLoS Pathog.* **10**, e1004264 (2014).
13. L. S. Mansfield *et al.*, C57BL/6 and congenic interleukin-10-deficient mice can serve as models of *Campylobacter jejuni* colonization and enteritis. *Infect. Immun.* **75**, 1099–1115 (2007).
14. R. E. Black, M. M. Levine, M. L. Clements, T. P. Hughes, M. J. Blaser, Experimental *Campylobacter jejuni* infection in humans. *J. Infect. Dis.* **157**, 472–479 (1988).
15. P. F. M. Teunis, A. Bonačić Marinović, D. R. Tribble, C. K. Porter, A. Swart, Acute illness from *Campylobacter jejuni* may require high doses while infection occurs at low doses. *Epidemics* **24**, 1–20 (2018).
16. J. P. van Spreeuwel *et al.*, *Campylobacter colitis*: Histological immunohistochemical and ultrastructural findings. *Gut* **26**, 945–951 (1985).
17. J. Mitobe *et al.*, An attenuated Shigella mutant lacking the RNA-binding protein Hfq provides cross-protection against Shigella strains of broad serotype. *PLoS Negl. Trop Dis.* **11**, e0005728 (2017).
18. O. Papapietro *et al.*, R-spondin 2 signalling mediates susceptibility to fatal infectious diarrhoea. *Nat. Commun.* **4**, 1898 (2013).
19. B. J. Saeedi *et al.*, HIF-dependent regulation of claudin-1 is central to intestinal epithelial tight junction integrity. *Mol. Biol. Cell* **26**, 2252–2262 (2015).
20. C. J. Kelly *et al.*, Crosstalk between microbiota-derived short-chain fatty acids and intestinal epithelial HIF augments tissue barrier function. *Cell Host Microbe* **17**, 662–671 (2015).
21. Y.-Y. Fan *et al.*, A bioassay to measure energy metabolism in mouse colonic crypts, organoids, and sorted stem cells. *Am. J. Physiol. Gastrointest. Liver Physiol.* **309**, G1–G9 (2015).
22. A. Y. Yu *et al.*, Temporal, spatial, and oxygen-regulated expression of hypoxia-inducible factor-1 in the lung. *Am. J. Physiology-Lung Cellular Mol. Physiol.* **275**, L818–L826 (1998).
23. F. Rivera-Chávez *et al.*, Depletion of butyrate-producing Clostridia from the gut microbiota drives an aerobic luminal expansion of Salmonella. *Cell Host Microbe* **19**, 443–454 (2016).
24. B. W. Stamps *et al.*, Exploring changes in the host gut microbiota during a controlled human infection model for *Campylobacter jejuni*. *Front. Cell Infect. Microbiol.* **11**, 702047 (2021).
25. T. Kanda *et al.*, *Enterococcus durans* TN-3 induces regulatory T cells and suppresses the development of dextran sulfate sodium (DSS)-induced experimental colitis. *PLoS ONE* **11**, e0159705 (2016).
26. C. C. Gillis *et al.*, Dysbiosis-associated change in host metabolism generates lactate to support Salmonella growth. *Cell Host Microbe* **23**, 54–64.e6 (2018).
27. R. Mercado-Lubo, M. P. Leatham, T. Conway, P. S. Cohen, *Salmonella enterica* serovar Typhimurium mutants unable to convert malate to pyruvate and oxaloacetate are avirulent and immunogenic in BALB/c mice. *Infect. Immun.* **77**, 1397–1405 (2009).
28. E. R. Hughes *et al.*, Microbial respiration and formate oxidation as metabolic signatures of inflammation-associated dysbiosis. *Cell Host Microbe* **21**, 208–219 (2017).
29. M. Stahl *et al.*, L-fucose utilization provides *Campylobacter jejuni* with a competitive advantage. *Proc. Natl. Acad. Sci. U.S.A.* **108**, 7194–7199 (2011).
30. D. Hofreuter, Defining the metabolic requirements for the growth and colonization capacity of *Campylobacter jejuni*. *Front. Cell Infect. Microbiol.* **4**, 137 (2014).
31. R. M. Exley *et al.*, Lactate acquisition promotes successful colonization of the murine genital tract by *Neisseria gonorrhoeae*. *Infect. Immun.* **75**, 1318–1324 (2007).
32. S. Lichtenegger *et al.*, Characterization of lactate utilization and its implication on the physiology of *Haemophilus influenzae*. *Int. J. Med. Microbiol.* **304**, 490–498 (2014).
33. K. N. Goodman, M. J. Powers, A. A. Crofts, M. S. Trent, D. R. Hendrixson, *Campylobacter jejuni* BumSR directs a response to butyrate via sensor phosphatase activity to impact transcription and colonization. *Proc. Natl. Acad. Sci. U.S.A.* **117**, 11715–11726 (2020).
34. M. T. Thomas *et al.*, Two respiratory enzyme systems in *Campylobacter jejuni* NCTC 11168 contribute to growth on L-lactate. *Environ. Microbiol.* **13**, 48–61 (2011).
35. P. K. Talukdar, N. M. Negretti, K. L. Turner, M. E. Konkel, Molecular dissection of the *Campylobacter jejuni* CadF and FlpA virulence proteins in binding to host cell fibronectin. *Microorganisms* **8**, 389 (2020).
36. P. M. Luethy *et al.*, Microbiota-derived short-chain fatty acids modulate expression of *Campylobacter jejuni* determinants required for commensalism and virulence. *mBio* **8**, e00407-17 (2017).
37. J. Coronel-Hernández *et al.*, Combination of metformin, sodium oxamate and doxorubicin induces apoptosis and autophagy in colorectal cancer cells via downregulation HIF-1α. *Front. Oncol.* **11**, 594200 (2021).
38. D. Zhang *et al.*, 2-Deoxyglucose reverses the promoting effect of insulin on colorectal cancer cells in vitro. *PLoS ONE* **11**, e0151115 (2016).
39. E. J. Guccione *et al.*, Transcriptome and proteome dynamics in chemostat culture reveal how *Campylobacter jejuni* modulates metabolism, stress responses and virulence factors upon changes in oxygen availability. *Environ. Microbiol.* **19**, 4326–4348 (2017).
40. C. C. Gillis *et al.*, Host-derived metabolites modulate transcription of Salmonella genes involved in L-lactate utilization during gut colonization. *Infect. Immun.* **87**, e00773-18 (2019).
41. P. Szczepanowski *et al.*, HP1021 is a redox switch protein identified in *Helicobacter pylori*. *Nucleic Acids Res.* **49**, 6863–6879 (2021).
42. P. Jaworski *et al.*, Structure and function of the *Campylobacter jejuni* chromosome replication origin. *Front. Microbiol.* **9**, 1533 (2018).
43. J. G. Johnson, J. A. Gaddy, V. J. DiRita, The PAS Domain-containing protein HeuR regulates heme uptake in *Campylobacter jejuni*. *mBio* **7**, e01691-16 (2016).
44. J. Jumper *et al.*, Highly accurate protein structure prediction with AlphaFold. *Nature* **596**, 583–589 (2021).
45. F. Corpet, Multiple sequence alignment with hierarchical clustering. *Nucleic Acids Res.* **16**, 10881–10890 (1988).
46. F. Rivera-Chávez, C. A. Lopez, A. J. Bäumler, Oxygen as a driver of gut dysbiosis. *Free Radic. Biol. Med.* **105**, 93–101 (2017).
47. Y. Litvak, M. X. Byndloss, A. J. Bäumler, Colonocyte metabolism shapes the gut microbiota. *Science* **362**, eaat9076 (2018).
48. L. P. Pral, J. L. Fachi, R. O. Corrêa, M. Colonna, M. A. R. Vinolo, Hypoxia and HIF-1 as key regulators of gut microbiota and host interactions. *Trends Immunol.* **42**, 604–621 (2021).
49. L. Rigottier-Gois, Dysbiosis in inflammatory bowel diseases: The oxygen hypothesis. *ISME J.* **7**, 1256–1261 (2013).
50. M. A. Smith, M. Finel, V. Korolik, G. L. Mendz, Characteristics of the aerobic respiratory chains of the microaerophiles *Campylobacter jejuni* and *Helicobacter pylori*. *Arch. Microbiol.* **174**, 1–10 (2000).
51. A. J. Van Alst, L. M. Demey, V. J. DiRita, *Vibrio cholerae* requires oxidative respiration through the bd-I and cbb3 oxidases for intestinal proliferation. *PLoS Pathog.* **18**, e1010102 (2022).
52. M. Hu *et al.*, Nucleolar c-Myc recruitment by a Vibrio T3SS effector promotes host cell proliferation and bacterial virulence. *EMBO J.* **40**, e105699 (2021).
53. V. Rivera-Amill, B. J. Kim, J. Seshu, M. E. Konkel, Secretion of the virulence-associated *Campylobacter* invasion antigens from *Campylobacter jejuni* requires a stimulatory signal. *J. Infect. Dis.* **183**, 1607–1616 (2001).
54. D. R. Samuelson *et al.*, The *Campylobacter jejuni* CiaD effector protein activates MAP kinase signaling pathways and is required for the development of disease. *Cell Commun. Signal.* **11**, 79 (2013).
55. P. Malik-Kale, C. T. Parker, M. E. Konkel, Culture of *Campylobacter jejuni* with sodium deoxycholate induces virulence gene expression. *J. Bacteriol.* **190**, 2286–2297 (2008).
56. X. Sun *et al.*, Microbiota-derived metabolic factors reduce *Campylobacteriosis* in mice. *Gastroenterology* **154**, 1751–1763.e2 (2018).
57. R. Dwivedi *et al.*, L-fucose influences chemotaxis and biofilm formation in *Campylobacter jejuni*. *Mol. Microbiol.* **101**, 575–589 (2016).
58. M. Stahl, J. Butcher, A. Stintzi, Nutrient acquisition and metabolism by *Campylobacter jejuni*. *Front. Cell Infect. Microbiol.* **2**, 5 (2012).
59. D. Carson *et al.*, *Citrobacter rodentium* induces rapid and unique metabolic and inflammatory responses in mice suffering from severe disease. *Cell Microbiol.* **22**, e13126 (2020).
60. M. Varatnitskaya, A. Degrossoli, L. I. Leichert, Redox regulation in host–pathogen interactions: Thiol switches and beyond. *Biol. Chem.* **402**, 299–316 (2021).
61. Z. Liu *et al.*, Differential thiol-based switches jump-start *Vibrio cholerae* pathogenesis. *Cell Rep.* **14**, 347–354 (2016).
62. R. Sinha *et al.*, gut_microbiome. nejcstopno/gut_microbiome. GitHub. https://github.com/nejcstopno/gut_microbiome. Deposited 8 August 2021.